

REGULAR PAPER

Development of an apparatus for Bragg coherent X-ray diffraction imaging, and its application to the three dimensional imaging of BaTiO₃ nano-crystals

To cite this article: Kenji Ohwada *et al* 2019 *Jpn. J. Appl. Phys.* **58** SLLA05

View the [article online](#) for updates and enhancements.

You may also like

- [Mechanical breakdown of bent silicon nanowires imaged by coherent x-ray diffraction](#)
Xiaowen Shi, Jesse N Clark, Gang Xiong et al.
- [Operando 3D imaging of defects dynamics of twinned-nanocrystal during catalysis](#)
Florian Meneau, Amélie Rochet, Ross Harder et al.
- [Bragg coherent diffraction imaging allowing simultaneous retrieval of three-dimensional shape and strain distribution for 40–500 nm particles](#)
Norihiro Oshime, Kenji Ohwada, Kento Sugawara et al.



Development of an apparatus for Bragg coherent X-ray diffraction imaging, and its application to the three dimensional imaging of BaTiO₃ nano-crystals

Kenji Ohwada^{1*}, Kento Sugawara¹, Tomohiro Abe², Tetsuro Ueno¹, Akihiko Machida¹, Tetsu Watanuki¹, Shintaro Ueno³, Ichiro Fujii³, Satoshi Wada³, and Yoshihiro Kuroiwa²

¹Synchrotron Radiation Research Center, Kansai Photon Science Institute, Quantum Beam Science Research Directorate, National Institutes for Quantum and Radiological Science and Technology (QST), SPring-8, 1-1-1 Kouto, Sayo, Hyogo 679-5148, Japan

²Graduate School of Science, Hiroshima University, Higashihiroshima, Hiroshima 739-8526, Japan

³Interdisciplinary Graduate School of Medical and Engineering, University of Yamanashi, 4-4-37 Takeda, Kofu 400-8510, Japan

*E-mail: ohwada.kenji@qst.go.jp

Received June 7, 2019; revised July 9, 2019; accepted August 5, 2019; published online August 23, 2019

We report the development of an apparatus for Bragg coherent X-ray diffraction imaging (Bragg-CDI) at BL22XU of SPring-8, and show some typical results of the three dimensional imaging of BaTiO₃ fine particles obtained using the apparatus. We studied two types of sample—particles with cubic-like shapes, and particles rich in curved surfaces. The shapes and sizes of the particles were successfully reconstructed, and are approximately consistent with results from scanning electron microscope (SEM) measurements. Further, details of the internal structure and reverse surface of the particles was obtained, information which is not available from SEM measurements. Our technique can currently be used to study particles as small as around 100 nm in size. Bragg-CDI is a powerful technique for investigating nanosized crystalline particles, and will open the door to studying particles located within devices such as multi-layered ceramic capacitors, inaccessible by electron beam techniques.
© 2019 The Japan Society of Applied Physics

1. Introduction

BaTiO₃ have attracted considerable scientific and industrial interests over the past few decades because they often show high permittivity, and have been used as key materials for dielectric devices such as multilayered ceramic capacitors (MLCCs). In recent years, demands on downsizing and higher capacitance of the MLCC devices require very thin dielectric layers with high permittivity. BaTiO₃ fine particles are used as materials for MLCC devices, with sizes which can be varied from several hundreds to tens of nanometers. Recently, not only the size^{1,2)} but also the shape^{3,4)} can be well controlled.

In the nanoscale regime, the dielectric properties of BaTiO₃ fine particles strongly depend on particle size (the so-called size effect).⁵⁻⁷⁾ It has also been reported that the physical properties depend on the sample synthesis condition. Figure 1 shows a typical example.^{8,9)} Generally, the dielectric constant of the BaTiO₃ fine particles increases as the average particle size decreases, with a rapid drop below a critical size. The reported critical sizes show a wide variation. This is believed to be due to non-uniform structures inside the particles.

At these sizes, the BaTiO₃ fine particles can no longer be treated as a simple bulk with tetragonal crystal system. The inset to Fig. 1 shows a schematic drawing of a proposed complex structure of BaTiO₃ fine particles. The crystal structure of the particle is composed of a core region with tetragonal crystal system and a shell region with cubic crystal system. A gradient lattice strain layer (GLSL)¹⁰⁾ bridges between the core and shell regions, and nanosized domains can exist in the core region.

To obtain a true picture of what is occurring within a BaTiO₃ fine particle, it is essential to precisely investigate the structure of individual single particles, including particle size, shape, global structure (such as domains and GLSL), and atomic structure, and compare this information with the physical properties of the same particle obtained for example

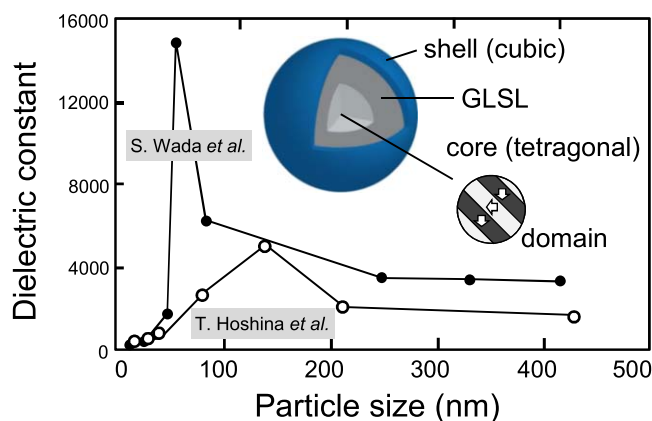


Fig. 1. (Color online) Average particle size dependence of dielectric constant. The values and the critical sizes strongly vary according to reports.^{8,9)} The inset shows a schematic drawing of the proposed composite structure of BaTiO₃ fine particles.

using a piezoresponse force microscope.^{11,12)} The conventional powder diffraction technique,^{13,14)} which gives the average atomic structure of whole particles is not sufficient. The atomic structure in a single particle can be now routinely determined in three dimensions by precise X-ray structural analysis.¹⁵⁾ The development of three dimensional visualization techniques for individual particles is in progress.

Coherent X-ray diffraction imaging (CDI)^{16,17)} is a powerful technique for visualizing the structure of nm to sub- μ m particles. CDI is a lens-less imaging technique which was rapidly developed following the availability of coherent X-ray light sources (3rd generation synchrotron light sources such as SPring-8). Several CDI techniques are in use at present,¹⁷⁾ however, the following approach is common to all techniques. If an object is illuminated by the coherent X-rays, the far-field diffracted wave is proportional to the Fourier transform of the object. This situation guarantees the possibility of image reconstruction. However, the diffracted

images are actually measured as a square of the Fourier transform, the phase information is lost, and therefore we cannot obtain the image by a simple inverse Fourier transform. This is called the phase problem. The image of the object can, however, be reconstructed by using a phase retrieval algorithm. The diffracted images must be sampled at a frequency finer than the Nyquist interval (this oversampling will be mentioned in Sect. 2).

Here we especially focus on the Bragg-CDI^{18–20} technique for visualizing individual fine particles. Bragg-CDI is a method dedicated to crystalline fine particles, where Bragg scattering can be obtained. In Bragg-CDI, a fine particle is illuminated by coherent X-rays and the diffraction patterns around a Bragg position are measured in three dimensions. Therefore, the three dimensional image of the fine particle can be obtained by the phase retrieval of the diffraction patterns. The retrieved amplitude and phase are related to the electron density and displacement/strain field of the crystal lattice in the fine particle, respectively.²⁰ Since the Bragg scattering profile and intensity are sensitive to degree of the decoherence of the crystal lattice, the Bragg-CDI method can therefore sensitively image the displacement or strain field in the fine particle. Since the orientation of particles is random in a powder, polycrystalline or ceramic sample, the Bragg-CDI technique should be a powerful tool for investigating individual particles in such samples. Because the Bragg peaks from individual particles can be separated in scattering space, the individual particles can be distinguished from their neighbors. Moreover, in most cases, three dimensional data can be obtained by changing the crystal angle by the order of 1 deg., which is an advantage over other CDI techniques.

Finally, we would like to note that, in the field of fine particles development, the scanning electron microscope (SEM) is frequently used for characterizing the particles. In this case, the shape and surface of the particles can be observed, however information on the internal structure (domains) and the shape and surface of the back of the particle can not be obtained. Furthermore, particles in devices, such as inside MLCC devices cannot be measured using electron beams. The use of (hard) X-rays can overcome its disadvantage.

The Bragg-CDI method and related techniques have been already developed in the United States (Advanced Photon Source) and applied to the study of various nanoparticles so far,^{21–24} however, no dedicated apparatus for Bragg-CDI exists in Japan. We are now aiming to construct an apparatus for investigating the structure of individual fine particles by the Bragg-CDI method. The Bragg-CDI method and the precise X-ray structural analysis of individual fine particles will be key techniques for obtaining a true picture of what is occurring in a single particle. In this report, the development of an apparatus for Bragg-CDI and three dimensional imaging of BaTiO₃ fine particles by the apparatus will be shown.

2. Experimental

The Bragg-CDI apparatus was developed on the coherent X-ray scattering station^{25–28} installed at BL22XU of SPring-8.²⁹

Figure 2 shows the schematic drawing of the present experimental setup. X-rays from an in-vacuum undulator

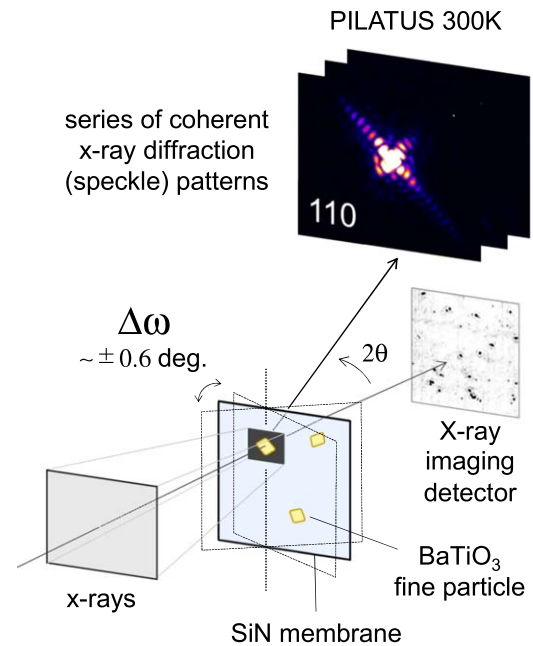


Fig. 2. (Color online) Schematic drawing of the setup for Bragg coherent X-ray diffraction imaging.

were monochromatized by a liquid-nitrogen-cooled Si(111) double-crystal monochromator. The energy was tuned to 8.7 keV ($\lambda = 1.425 \text{ \AA}$). Fine particles were mounted on a SiN membrane with a thickness of 200 nm (X05-A200Q25, Filgen, Inc.). The X-ray coherency was not disturbed by passing through this membrane. The particles on the SiN membrane were observed by a high-resolution lens-coupled X-ray imaging detector³⁰ XRDCH-S0-C1 (SIGMAKOKI Co., LTD.). As shown in Fig. 2, we could confirm that the particles were dispersively supported on the SiN membrane. In this direct imaging case, a large-area direct X-ray beam of larger than $300 \times 300 \mu\text{m}^2$ was used, without focusing.

For Bragg-CDI, the X-rays were focused by a refractive lens (Karlsruhe Institute of Technology)³¹ to 6×10 (vertical \times horizontal) μm^2 , with a focal length of 3.835 m. A BaTiO₃ fine particle on the SiN membrane is illuminated by the focused X-rays and the diffracted X-rays were collected by a two-dimensional photon counting detector PILATUS 300K (DECTRIS Ltd.). The pixel size of the detector was $172 \times 172 \mu\text{m}^2$ (P^2). The detector was positioned at 1.6 m (R) downstream from the sample. The most intense 110 Bragg reflection, with a scattering angle (2θ) of approximately 29.2 deg., was chosen for the present measurements. A typical coherent X-ray diffraction pattern is shown in Fig. 2. One can clearly observe speckles around the center, and, in general, we call the coherent X-ray diffraction (scattering) patterns speckle³² patterns. We collected three dimensional speckle patterns around the 110 Bragg position by changing the Bragg angle (ω scan) by ± 0.6 deg. with a 0.01 deg. step.

By using the three dimensional Bragg diffraction data, we reconstructed three dimensional images of BaTiO₃ fine particles. The phase retrieval of the observed diffraction patterns was carried out with a series of hybrid input output and error reduction algorithms,³³ which are frequently used in CDI. Most of the iterative operations converged after ~ 1000 cycles. The initial phase was set as random, and we

tried various initial phases and confirmed that each reconstructed image was approximately similar.

The above experimental setting satisfies the following three conditions required for the phase retrieval of the observed diffraction patterns. (i) The particle size (a) is within the transverse and longitudinal coherence lengths ($\xi_T^V \geq a$, $\xi_T^H \geq a$ and $\xi_L \geq a$). The transverse coherence lengths at the sample position are $\xi_T^V \xi_T^H \sim 6 \times 1$ (vertical \times horizontal) μm^2 and the longitudinal coherence length, directly relating to the energy resolution of the monochromator ($\Delta E/E \sim 10^{-4}$), is approximately $\xi_L \sim 1 \mu\text{m}$ (ii) Observed diffraction patterns are over-sampled [speckle size $(\lambda R/a)^2 \geq 2P^2$]. (iii) The diffraction is far-field diffraction ($R \gg a^2/\lambda$).

Three types of BaTiO_3 fine particles were prepared: cube-like shaped particles with an average size ($=a$) of 300 nm and 100 nm (BT-Y1 and BT-Y2, respectively, University of Yamanashi³⁾ and particles with rich curved surfaces (BT-S, Sakai Chemical Industry Co., Ltd.).

3. Results and discussion

In this section, we show some typical imaging results obtained by the Bragg-CDI method.

Figure 3 shows a result obtained from a particle of the BT-Y1 sample. As shown in Fig. 3(a), the scattering pattern is crisscrossed and very well reflects the Fourier transform of the cube shape. The reconstructed image shown in Fig. 3(b) actually shows that the shape of the particle is almost cubic, with a size of approximately 300 nm in the longitudinal direction. Figures 3(c) and 3(d) show cross-sectional images of the electron density and the phase corresponding to the strain, cut by the blue plane in Fig. 3(b). The white square line is the “support” used for the phase retrieval as the real space constraint; with no electron density outside of the support. The dotted black lines in Figs. 3(c) and 3(d) are a guide to the eyes. The phase inside the particle is almost uniform around zero, reflecting the presence of the particle. The phase outside the particle, on the other hand, is randomly distributed from $-\pi$ to π indicating no object in this outer region. One can see some stripes in Figs. 3(c) and 3(d). The origin of this pattern is not clear at present and this characteristic pattern is considered to be due to an induced structure during the particle growth, a trace of the ferroelastic domain, or a genuine artifact. Figure 3(e) shows a SEM image of the BT-Y1 sample. Cubic-like shaped particles are observed. Our imaging result shown in Fig. 3(b) is consistent with the SEM image. In addition to the shape and size of the particle, we have observed the internal structure of the particle.

Figure 4 shows a result obtained from a particle of the BT-S sample. As shown in Fig. 4(a), the scattering pattern is more complicated than that of Fig. 3(a). The reconstructed image shown in Fig. 4(b) actually shows that the shape of the particle is rich in curved surfaces. Figures 4(c) and 4(d) show the cross-sectional image of the electron density and the phase, cut by the blue plane in Fig. 4(b). The white circle line shows the support. The dotted black lines in Figs. 4(c) and 4(d) are for a guide to the eyes. The cross section of the particle is approximately pentagonal, and the size reaches 500 nm in the longitudinal direction. Similar to Fig. 3, the origin of the nonuniformity of the density seen in Fig. 4(c) is not clear at present. The phase seen in Fig. 4(d) shows a

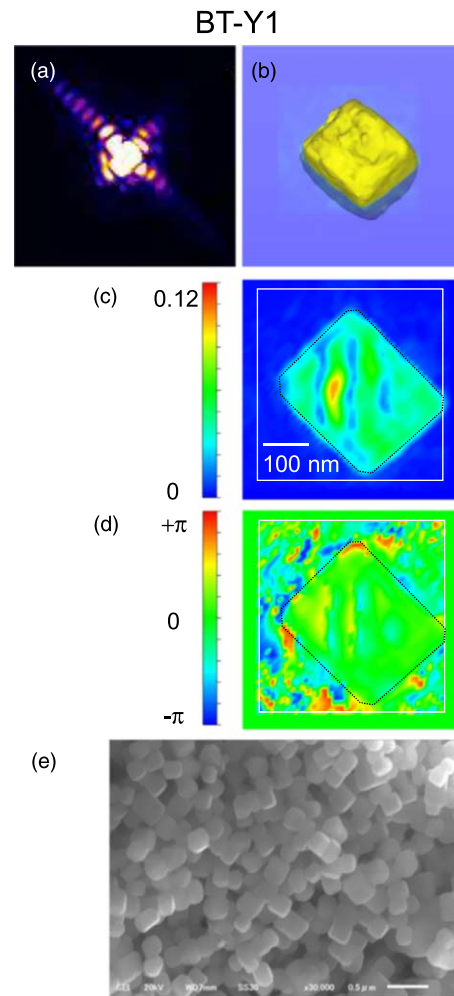


Fig. 3. (Color online) (a) Single recorded diffraction pattern for a particle from the BT-Y1 sample. (b) Reconstructed three dimensional image of the particle. (c) and (d) show cross-sectional image of the electron density and the phase (strain), cut by the blue plane in (b). (e) SEM image of the BT-Y1 sample. The white bar corresponds to 500 nm. Figure (a) was drawn using ImageJ,³⁴⁾ and figures (b)–(d) were drawn using VESTA.³⁵⁾

stress concentration near the two edges at the top right, which gradually changes from top right to bottom left. Figure 4(e) shows the SEM image of the BT-S sample. A particle similar in shape to Fig. 4(b) can be observed. Our result is thus well consistent with the obtained SEM image. In addition to the shape and size of the particle, we have observed the internal structure of the particle as well.

Reconstructed images of additional particles are shown in Fig. 5. In the case of this figure, the phase value is limited to be positive during the phase retrieval treatment for good convergence. Figure 5(a) shows the three dimensional image of a particle from the BT-Y1 sample. The shape is almost cubic, and the size is approximately 240 nm. We also successfully managed to recover the shape of a particle from the BT-Y2 sample, as shown in Fig. 5(b). The reconstructed image is still coarse and the result requires higher data quality. Nevertheless, the shape can be identified to be almost cubic, and the size is also measured to be approximately 130 nm. Thus, the present Bragg-CDI method works very well to obtain the structural character of each individual particle. Figure 5(c) shows the three dimensional shape of a particle from the BT-S sample. The size is approximately 350 nm, and the shape is rich in curved surface.

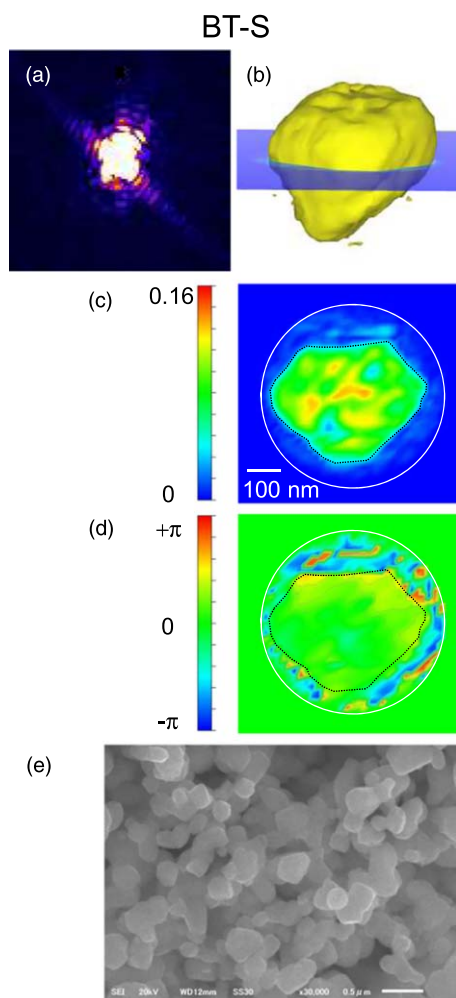


Fig. 4. (Color online) (a) Single recorded diffraction pattern for a particle from the BT-S sample. (b) Reconstructed three dimensional image of the particle. (c) and (d) show cross-sectional images of the electron density and the phase (strain), cut by the blue plane in (b). (e) SEM image of the BT-S sample. The white bar corresponds to 500 nm. Figure (a) is drawn using ImageJ,³⁴⁾ and figures (b)–(d) are drawn using VESTA.³⁵⁾

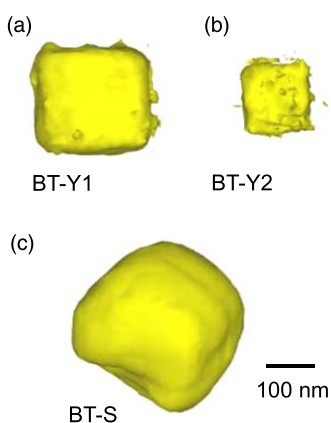


Fig. 5. (Color online) The obtained three dimensional images of particles from (a) BT-Y1, (b) BT-Y2 and (c) BT-S samples. The Figs. were drawn using VESTA.³⁵⁾

4. Summary

We have reported the development of an apparatus for Bragg-CDI at BL22XU of SPring-8, and have shown some typical results of the three dimensional imaging of BaTiO₃ fine particles obtained using the apparatus. We have studied two

types of sample—particles with cubic-like shapes, and particles rich in curved surfaces, with a size of typically 300 nm. The shapes and sizes of the particles were successfully reconstructed, and are approximately consistent with results from SEM measurements. Further, details of the internal structure and reverse surface of the particles was obtained, information which is not available from SEM measurements. Our technique can currently be used to study particles as small as around 100 nm (or smaller) in size. Bragg-CDI is a powerful technique for investigating nano-sized crystalline particles, and will open the door to studying particles located within devices such as MLCCs, inaccessible by electron beam techniques.

Acknowledgments

We would like to thank Dr. H. Kono (QST) for discussions about phase retrieval, and providing a model program. We would like to thank Prof. M. Takesada (Hokkaido Univ.) and J. R. Harries (QST) for discussion and comments. We thank Karlsruhe Institute of Technology/Institute of Microstructure Technology and ASICON Tokyo Ltd. for realizing the compound refractive lenses for the present synchrotron X-ray scattering experiments. We thank Japan Synchrotron Radiation Research Institute (JASRI) for providing a chance for use the PILATUS 300 K detector. This work was partly supported by JSPS Grant-in-Aid for Scientific Research (B) (Grant No. 19H02618). The synchrotron X-ray scattering experiment was performed at SPring-8 with the approval of JASRI (Proposal Nos. 2017B3761, 2018A3761, 2018B3761, 2019A3761).

ORCID iDs

Ichiro Fujii  <https://orcid.org/0000-0003-0207-6415>

- 1) T. Karaki, K. Yan, T. Miyamoto, and M. Adachi, *Jpn. J. Appl. Phys.* **46**, L97 (2007).
- 2) S. Wada, S. Kondo, C. Moriyoshi, and Y. Kuroiwa, *Jpn. J. Appl. Phys.* **47**, 7612 (2007).
- 3) S. Wada, A. Nozawa, M. Ohno, H. Kakemoto, T. Tsurumi, Y. Kameshima, and Y. Ohba, *J. Mater. Sci.* **44**, 5161 (2009).
- 4) K. Kato, K. Mimura, F. Dang, H. Imai, S. Wada, M. Osada, H. Haneda, and M. Kuwabara, *J. Mater. Res.* **44**, 2932 (2013).
- 5) G. Arlt, D. Hennings, and G. de With, *J. Appl. Phys.* **58**, 1619 (1985).
- 6) K. Ishikawa, K. Yoshikawa, and N. Okada, *Phys. Rev. B* **37**, 5852 (1988).
- 7) T. Yamamoto, K. Urabe, and H. Banno, *Jpn. J. Appl. Phys.* **32**, 4272 (1993).
- 8) S. Wada, H. Yasuno, T. Hoshina, S.-M. Nam, H. Kakemoto, and T. Tsurumi, *Jpn. J. Appl. Phys.* **42**, 6188 (2003).
- 9) T. Hoshina, *J. Ceram. Soc. Jpn.* **121**, 156 (2013).
- 10) T. Hoshina, S. Wada, Y. Kuroiwa, and T. Tsurumi, *Appl. Phys. Lett.* **93**, 192914 (2008).
- 11) S. Ray, Y. V. Kolen'ko, D. Fu, R. Gallage, N. Sakamoto, T. Watanabe, M. Yoshimura, and M. Itoh, *Small* **2**, 1427 (2006).
- 12) H. Fujisawa, Y. Seioh, M. Kume, and M. Shimizu, *Jpn. J. Appl. Phys.* **47**, 7505 (2008).
- 13) S. Aoyagi, Y. Kuroiwa, A. Sawada, I. Yamashita, and T. Atake, *J. Phys. Soc. Jpn.* **71**, 1218 (2002).
- 14) Y. Kuroiwa, S. Aoyagi, A. Sawada, H. Ikawa, I. Yamashita, N. Inoue, and T. Atake, *J. Therm. Anal. Calorim.* **69**, 933 (2002).
- 15) N. Yasuda et al., *J. Synchrotron Radiat.* **16**, 352 (2009).
- 16) J. Miao, P. Charalambous, J. Kirz, and D. Sayre, *Nature* **400**, 342 (1999).
- 17) J. Miao, T. Ishikawa, I. K. Robinson, and M. M. Murnane, *Science* **348**, 530 (2015).
- 18) I. K. Robinson, I. A. Vartanyants, G. J. Williams, M. A. Pfeifer, and J. A. Pitney, *Phys. Rev. Lett.* **87**, 195505 (2001).
- 19) M. A. Pfeifer, G. J. Williams, I. A. Vartanyants, R. Harder, and I. K. Robinson, *Nature* **442**, 63 (2006).
- 20) I. Robinson and H. Ross, *Nat. Mater.* **8**, 291 (2009).

- 21) S. O. Hruszkewycz, M. J. Highland, M. V. Holt, D. Kim, C. M. Folkman, C. Thompson, A. Tripathi, G. B. Stephenson, S. Hong, and P. H. Fuoss, *Phys. Rev. Lett.* **110**, 177601 (2013).
- 22) W. Cha, A. Ulvestad, M. Allain, V. Chamard, R. Harder, S. J. Leake, J. Maser, P. H. Fuoss, and S. O. Hruszkewycz, *Phys. Rev. Lett.* **117**, 225501 (2016).
- 23) D. Karpov, Z. Liu, T. dos Santos Rolo, R. Harder, P. V. Balachandran, D. Xue, T. Lookman, and E. Fohntung, *Nat. Commun.* **8**, 280 (2017).
- 24) A. Ulvestad et al., *Nat. Mat.* **16**, 565 (2017).
- 25) K. Ohwada, K. Namikawa, J. Mizuki, S. Simomura, H. Nakao, K. Itoh, M. Matsushita, Y. Yoneda, Y. Murakami, and K. Hirota, *Trans. Mater. Res. Soc. Jpn.* **32**, 7 (2007).
- 26) K. Ohwada, J. Mizuki, K. Namikawa, M. Matsushita, S. Shimomura, H. Nakao, and K. Hirota, *Phys. Rev. B* **83**, 224115 (2011).
- 27) K. Ohwada, J. Mizuki, M. Matsushita, and K. Namikawa, *Phys. Rev. B* **90**, 104109 (2014).
- 28) K. Ohwada, D. Shimizu, J. Mizuki, K. Fujiwara, T. Nagata, N. Ikeda, H. Ohwa, N. Yasuda, and K. Namikawa, *Ferroelectrics* **513**, 16 (2017).
- 29) T. Shobu, K. Tozawa, H. Shiwaku, H. Konishi, T. Inami, T. Harami, and J. Mizuki, *AIP Conf. Proc.* **879**, 902 (2007).
- 30) T. Kameshima, A. Takeuchi, K. Uesugi, T. Kudo, Y. Kohmura, K. Tamasaku, K. Muramatsu, T. Yanagitani, M. Yabashi, and T. Hatsui, *Opt. Lett.* **44**, 1403 (2019).
- 31) C. Krywka, A. Lastgđ, F. Marschall, O. Markus, S. Georgi, M. Muller, and J. Mohr, *AIP Conf. Proc.* **1764**, 020001 (2016).
- 32) M. Sutton, S. G. J. Mochrie, T. Greytak, S. E. Nagler, L. E. Berman, G. A. Held, and G. B. Stephenson, *Nature* **352**, 608 (1991).
- 33) J. R. Fienup, *Appl. Opt.* **21**, 2758 (1982).
- 34) M. D. Abramoff, P. J. Magelhaes, and S. J. Ram, *Biophotonics Int.* **11**, 36 (2004).
- 35) K. Momma and F. Izumi, *J. Appl. Crystallogr.* **44**, 1272 (2011).